Available online at www.sciencedirect.com
SCIENCE DIRECT®
International Journal of Heat and Mass Transfer 47 (2004) 2653–2667
International Journal of HEAT and MASS TRANSFER
www.elsevier.com/locate/ijhmt

Heat and mass transfer during absorption of ammonia vapour by $LiNO_3$–NH_3 solution droplets

M. Venegas [a,1], M. Izquierdo [b,*,1], P. Rodríguez [a,1], A. Lecuona [a,1]

[a] Departamento de Ingeniería Térmica y de Fluidos, Universidad Carlos III de Madrid, Avda. Universidad, 30, 28911 Leganés, Madrid, Spain

[b] Instituto de Ciencias de la Construcción Eduardo Torroja (CSIC), C. Serrano Galvache, s/n, 28033 Madrid, Spain

Received 5 June 2003; received in revised form 2 December 2003

Abstract

In this paper the simultaneous mass and heat transfer processes taking place during the absorption of ammonia vapour by lithium nitrate–ammonia solution droplets is numerically simulated. The low-pressure and high-pressure absorbers of a double-stage absorption system are considered. Results obtained are compared with Newman model for mass transfer. Simulation shows that droplets analysed, with diameter equal to 60 and 100 μm, follow Newman model for mass transfer. Droplets achieve the equilibrium state in an approximate dimensionless time equal to 0.5, that corresponds to times lower than 1 s. Effect of subcooling on absorption is evaluated. Results obtained are important for the design of spray absorbers of absorption refrigeration systems.

1. Introduction

The development of absorption refrigeration technology is basically related with the heat and mass transfer research in the absorption machine components. Also, it is already known that mass transfer is the main constraint for increasing performance and reducing dimensions of absorption machines. Absorption refrigeration systems commonly use laminar falling film absorbers. However, other absorption methods have shown their potential for reducing the heat and mass transfer area and, as a result, the absorber dimensions. These methods include spray and bubble absorption. For theoretical and experimental studies about spray and bubble absorption the works [1–8] and [9–16] can be consulted, respectively.

The simultaneous heat and mass transfer in droplets is a complex process where the mass and energy conservation equations must be solved simultaneously. To date analytical models that predict the simultaneous variation of the concentration and temperature in droplets, considering their size, velocity, internal circulation, flow pattern, etc. do not exist. If all these factors could be accurately considered the characteristics of the heat and mass transfer in individual droplets would correctly predict the global process that takes place in spray absorbers of absorption refrigeration systems. To date several studies have been published that analyse the heat and/or mass transfer in droplets. A classification of these works follows:

Analytical models for individual heat or mass transfer. The works [17–25] can be found in the literature. These models have mainly application in chemical engineering and predict the heat or mass transfer in droplets in specific cases.

Experimental studies on mass transfer. In addition to the theoretical models for mass transfer in droplets many experimental works are reported. For example, [26–28] for the absorption of CO_2 in water and [29] for the absorption of CO_2 in a solution of carbonate and sodium bicarbonate.

Numerical solutions for individual heat or mass transfer. The main limitation of analytical models is given by the simplifications made during the solution

* Corresponding author. Fax: +34-91-871-3248.
E-mail address: mizquierdo@ietcc.csic.es (M. Izquierdo).
[1] Unidad Asociada de Ingeniería Térmica y de Fluidos CSIC-UC3M.

0017-9310/$ - see front matter © 2004 Elsevier Ltd. All rights reserved.
doi:10.1016/j.ijheatmasstransfer.2003.12.014

Nomenclature

a	constant in thermodynamic equilibrium equation
C_p	specific heat
COP	coefficient of performance
d	droplet diameter (mm)
D	diffusion coefficient (m^2/s)
d_0	atomiser hole diameter
E	dimensionless approach to equilibrium
Fo	Fourier number
i	radial coordinate in droplet discretisation
j	angular coordinate in droplet discretisation
k	thermal conductivity
L	latent heat
m	mass flux ($kg/m^2\,s$)
ncita	points number in angular direction
nr	points number in radial direction
p	volumetric mass flux ($kg/m^3\,s$)
P	pressure
Pe	Peclet number
Pe^J	modified Peclet number
q	heat flux (kW/m^2)
r	radial distance
r	position vector
$\bar{r}$	dimensionless radial distance
R	droplet radius
Re	Reynolds number
s	constant in thermodynamic equilibrium equation
SMD	Sauter Mean Diameter
t	time
t_c	circulation time (s)
t_d	diffusion time (s)
T	temperature
$\overline{T}$	dimensionless temperature
u	droplet velocity
$\bar{u}$	droplet velocity vector
u_c	circulation velocity (m/s)
x	refrigerant mass fraction in the liquid phase (kg/kg)
$\bar{x}$	dimensionless refrigerant mass fraction in the liquid phase
ΔP	pressure drop
$\Delta\bar{r}$	grid step in the radial direction
ΔT	temperature increase
Δx	concentration increase
$\Delta\theta$	grid step in the angular direction
$\Delta\tau$	time step

Greek symbols

α	thermal diffusivity
ϕ	spherical coordinate angle
γ	liquid and vapour viscosity ratio
η	velocity lost coefficient
φ	stream function
μ	viscosity
ν	cinematic viscosity
θ	angle in Fig. 3
ρ	density
ρ_{amon}	ammonia mass per unit of solution volume (kg/m^3)
σ	surface tension
τ	dimensionless time

Subscripts

c	continuous phase
d	disperse phase
eq	thermodynamic equilibrium
i	radial coordinate
j	angular coordinate
0	initial instant
r	radial direction
sol	solution
θ	θ direction

Superscript

n	iteration number

of equations, which make the models only valid for special cases. For this reason several authors have solved numerically more complex cases for which analytical solutions do not exist. General solutions obtained by [30–38] belong to these works. The problem of mass transfer in specific cases also has been numerically studied. For example, the absorption of SO_2 by water droplets [39,40], of HCl by droplets of diluted sulphuric acid [41], the absorption of SO_2 by droplets of diluted lime [42] and the absorption of SO_2 and HCl by water droplets [43].

Analytical models for the simultaneous heat and mass transfer. Respect to the problem of simultaneous heat and mass transfer in the literature appears the analytical model developed by Nakoryakov and Grigoreva [44]. This model is valid for static droplets and does not consider the angular variation of the concentration and temperature inside the droplet.

Experimental studies on simultaneous heat and mass transfer. Experimental studies on simultaneous heat and mass transfer are scarce. In [1,2] authors use the lithium bromide–water solution. Their work was intended to verify experimentally the correlation obtained by [44]. Results obtained show a great discrepancy for Fourier numbers in the range $Fo < 0.01$ and $Fo > 0.04$. Ryan [4] and Ryan et al. [5] also made several experiments using

the lithium bromide–water solution. In [5] authors conclude that the model developed by Newman [17] is suitable for predicting the mass transfer to dispersed droplets. Some experimental works using other pairs also have been published. For example, Fenton et al. [45] analyses the absorption of ammonia by pure water droplets and Summerer et al. [6] and Flamensbeck et al. [7] study the heat and mass transfer between binary or ternary mixtures and water.

Numerical solutions for simultaneous heat and mass transfer. Due to the non-existence of suitable correlations to describe the simultaneous heat and mass transfer, some authors have used numerical procedures to simulate these processes. At present reported papers include those of Morioka et al. [3] and Lu et al. [46]. In both cases the absorption of water vapour by lithium bromide–water solution droplets is analysed.

Considering the cases reported in the literature, it could be concluded that analytical models for the simultaneous heat and mass transfer in moving droplets do not exist. This process takes place inside spray absorbers of absorption refrigeration machines. On the other hand, for the case of the lithium nitrate–ammonia solution droplets no studies, neither experimental nor theoretical, have been reported.

Taking into account the need for calculating the absorption of refrigerant vapour by solution droplets, aiming to the design of real spray absorption systems, in this paper a model for the simultaneous heat and mass transfer in lithium nitrate–ammonia solution droplets is presented. The analytical model is numerically solved for a sample case of double-stage absorption system that may be found in real spray absorbers. Results obtained are compared with those given by Newman model for mass transfer.

2. Absorption system

The double-stage absorption cycle considered appears in Fig. 1. The absorption system is divided into two stages, namely high-pressure (HPA) and low-pressure (LPA) absorbers. One generator (HPG or LPG), one absorber and one solution heat exchanger compose each stage. Condenser (C) is located in the high-pressure zone. Vapour condensed there goes to the evaporator (E) situated in the low-pressure zone producing here the cooling effect.

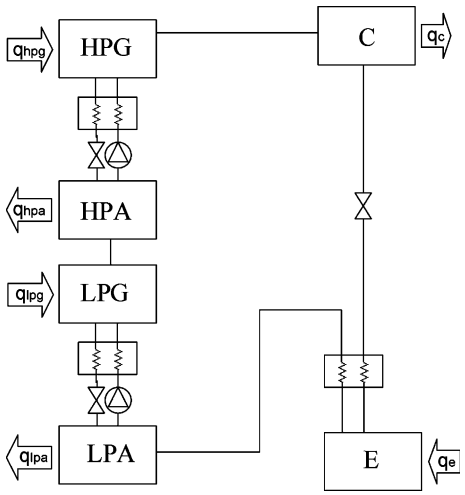

Fig. 1. Scheme of the double-stage absorption system.

Due to the difference of solution concentration in both stages, ammonia vapour is generated and the cooling effect is obtained using lower generation temperatures than those required in single effect cycles. Refs. [47,48] present the thermodynamic relations used for modelling this system, and results about COP and generation temperatures required for each absorption, condensation and evaporation temperature.

The case selected for the numerical simulation corresponds to the worst operating conditions of the double-stage absorption machine analysed in [47,48]. All the physical properties are assumed to be constant in the range considered for pressures and temperatures. Solution and vapour properties in the low-pressure absorber and high-pressure absorber appear in Tables 1 and 2. These properties are taken from Infante Ferreira [10,49], ASHRAE [50], IIAR [51] and Kusaka [52].

3. Spray characterisation

When spray absorption is used the mass and heat transfer processes are divided in separate apparatus and the absorption occurs inside the adiabatic chamber (Fig. 2). The absorption heat is extracted using liquid–liquid

Table 1
Lithium nitrate–ammonia solution properties

Absorber	x (%)	T (°C)	P (bar)	ρ_d (kg m^{-3})	μ_d (Pa s)	C_p (kJ kg^{-1} K^{-1})	σ (N m^{-1})	α (m^2 s^{-1})	D (m^2 s^{-1})
Low-pressure absorber	36.7	40	2.36	1132	7.62×10^{-3}	2.620	0.052	5.1×10^{-7}	0.74×10^{-9}
High-pressure absorber	50	40	6.49	989	7.94×10^{-4}	3.121	0.050	4.2×10^{-7}	1.62×10^{-9}

Table 2
Ammonia vapour properties

Absorber	T (°C)	ρ_c (kg m^{-3})	μ_c (Pa s)	L (kJ kg^{-1})
Low-pressure absorber	10	1.76	9.8×10^{-6}	1.31×10^{3}
High-pressure absorber	85	3.77	12.3×10^{-6}	1.23×10^{3}

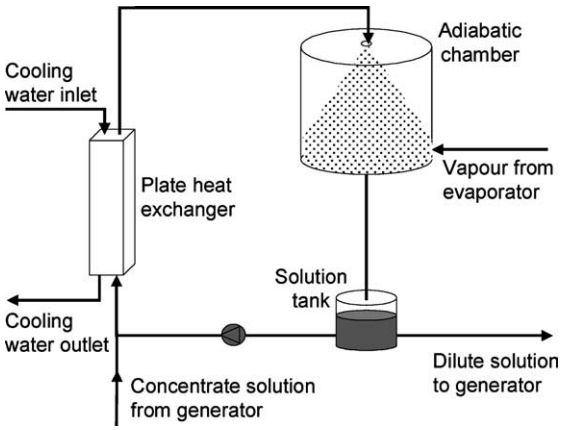

Fig. 2. Scheme of the spray absorber configuration.

plate heat exchangers. The reduction of droplets diameter as much as possible is convenient with the objective of increasing the interfacial area and consequently the mass transfer rate. It will translate in smaller absorber dimensions and lower cost. In the present case pressure atomisers will be considered, because pressure lift in ammonia absorption machines is sufficient to produce atomisation. According to Lefebvre [53] a pressure difference of 1.5 bar is sufficient. The velocity of the fluid leaving the atomiser is calculated through

$$u = \eta\sqrt{\frac{2\Delta P}{\rho_{sol}}} \tag{1}$$

where the velocity loss coefficient η is obtained from [54] as a function of the Reynolds number. To calculate the Sauter Mean Diameter (SMD) of the generated droplets the following relation proposed by Lefebvre [53] is used:

$$\mathrm{SMD} = 3330 d_0^{0.3}\mu_d^{0.07}\rho_d^{-0.648}\sigma^{-0.15}u^{-0.55}\mu_c^{0.78}\rho_c^{-0.052} \tag{2}$$

Using Eqs. (1) and (2) and data from Tables 1 and 2, the SMD of the droplets leaving the atomisers can be estimated. These correspond to 60 μm in the low-pressure absorber and 100 μm in the high-pressure absorber. Very small diameters have been considered with the objective of increasing the interfacial area between solution and vapour and, as a result, increasing the mass transfer rate. In this study it is supposed that both absorbers have a conical section with maximum diameter equal to 30 cm. The counter-current vapour flows with a velocity equal to 0.12 m/s (0.26 m/s) in the low-pressure absorber (high-pressure absorber).

When aerodynamic forces balance gravitational forces acting over a droplet, it achieves a uniform movement and moves at its terminal velocity. For conditions given the terminal velocity of the droplets is equal to 0.17 m/s (0.29 m/s) in the low-pressure absorber (high-pressure absorber). Reynolds numbers correspond to 1.4 and 6.2, respectively. Terminal velocities and Reynolds number obtained are used in the next sections to simulate the heat and mass transfer processes taking place inside the absorption chambers.

4. Simulation model for absorption of ammonia vapour by lithium nitrate–ammonia droplets

A single spherical droplet of lithium nitrate–ammonia solution of radius R translating and experimenting absorption of ammonia vapour is considered (Fig. 3). Also the following hypotheses are taken into account:

- Radius of the droplet is constant.
- Heat release occurs at the interface between the droplet and the surrounding vapour. Conduction and convection processes control the heat transfer inside the droplet.
- Droplet keeps the spherical form during its fall.
- Coalescence and collisions between droplets are not considered.
- Contribution to mass transfer of the liquid film falling by the absorber wall is insignificant.
- No heat is transferred into/from the vapour phase.

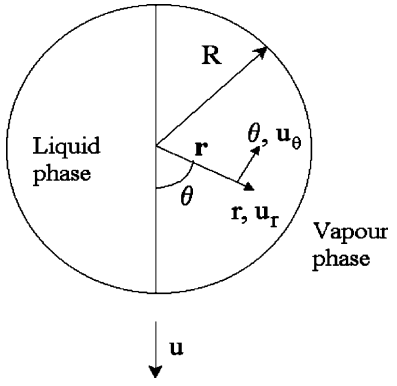

Fig. 3. Droplet physical model.

4.1. Heat and mass transfer model

Ammonia concentration profile in the liquid phase can be described through the continuity equation [55,56]:

$$-\nabla\cdot(\rho_{\mathrm{d}}D\nabla x)+\nabla\cdot(\rho_{\mathrm{amon}}\bar{u})+\frac{\partial\rho_{\mathrm{amon}}}{\partial t}-p=0 \tag{3}$$

In Eq. (3) the mass increase in the first term is due to the concentration gradient existing and in the second term due to the apparent movement of the fluid. The third term corresponds to the mass accumulation velocity inside the control volume. The source term p corresponds to the ammonia chemical production. In the present case ammonia production does not occur.

When solution is dispersed in droplets inside an adiabatic chamber through pressure atomisers, small variations in temperature and concentration occur. Thus, density and diffusion coefficient can be considered constants (Table 1). Previous numerical works developed about absorption of refrigerant vapour by solution droplets [3,46] also include this consideration. Eq. (3) is reduced to

$$-D\nabla^2x+\bar{u}\cdot\nabla x+\frac{\partial x}{\partial t}=0$$

This equation expressed in spherical coordinates and considering symmetry in ϕ direction takes the following form:

$$\frac{\partial x}{\partial t}+u_r\cdot\frac{\partial x}{\partial r}+\frac{u_\theta}{r}\frac{\partial x}{\partial\theta}=D\left(\frac{\partial^2x}{\partial r^2}+\frac{2}{r}\frac{\partial x}{\partial r}+\frac{\cot\theta}{r^2}\frac{\partial x}{\partial\theta}+\frac{1}{r^2}\frac{\partial^2x}{\partial\theta^2}\right) \tag{4}$$

The first term in the left side of Eq. (4) corresponds to the ammonia accumulation rate inside the droplet and the second and third terms to the convective concentration increase in the radial and angular directions, respectively, due to the velocity field. The right term of Eq. (4) corresponds to the concentration variation in the radial and angular directions due to the molecular diffusion inside the droplet.

Performing a similar analysis the energy conservation equation in spherical coordinates is obtained:

$$\frac{\partial T}{\partial t}+u_r\cdot\frac{\partial T}{\partial r}+\frac{u_\theta}{r}\frac{\partial T}{\partial\theta}=\alpha\left(\frac{\partial^2T}{\partial r^2}+\frac{2}{r}\frac{\partial T}{\partial r}+\frac{\cot\theta}{r^2}\frac{\partial T}{\partial\theta}+\frac{1}{r^2}\frac{\partial^2T}{\partial\theta^2}\right) \tag{5}$$

The first term in the left side of Eq. (5) corresponds to the temperature variation with time inside the droplet and the second and third terms to the temperature increase in the radial and angular directions, respectively, due to convection effect. The right term of Eq. (5) corresponds to the temperature variation in the radial and angular directions due to conduction.

Initial and boundary conditions in the case of absorption of refrigerant vapour by solution droplets are the followings:

Initial conditions

for $t=0$,

$$x=x_0 \text{ and } T=T_0 \quad \text{for all } r \tag{6}$$

Boundary conditions

at $r=0$,

$$\frac{\partial x}{\partial r}=\frac{\partial T}{\partial r}=0 \quad \text{for } t>0 \tag{7}$$

at $r=R$,

$$x=x_{\mathrm{eq}} \text{ and } T=T_{\mathrm{eq}} \quad \text{for } t>0 \tag{8}$$

At constant pressure, the relation between temperature and concentration for a mixture at saturated equilibrium can be approximated through a linear relation, with a and s constants [2,3,44,46]:

$$x_{\mathrm{eq}}=a\cdot T_{\mathrm{eq}}+s \tag{9}$$

Constants a and s take the values in Table 3 for the operating conditions of the double-stage absorption refrigeration machine considered.

Another boundary condition is that the heat flux at the droplet surface is proportional to the mass absorbed of refrigerant vapour:

$$q=-L\cdot m \tag{10}$$

or the same relation:

$$k\left(\frac{\partial T}{\partial r}\right)_{r=R}=-L\cdot\rho D\left(\frac{\partial x}{\partial r}\right)_{r=R}$$

Eq. (10) relates the mass and heat equations and brings on the problem to a non-isothermal one. This equation is based on the considerations that absorption heat release occurs only at the droplet surface and that no heat is transferred into/from the vapour phase. In previous numerical works, developed for droplets absorption processes [3,46], no heat transfer to/from the vapour has been considered. In Habib and Wood [57] an analysis of the simultaneous heat and mass transfer inside a vertical tubular absorber of 1 m length using the lithium bromide–water solution is presented. The authors conclude that significant heat is transferred to the vapour.

Table 3
Parameters for Eq. (9)

Absorber	P (bar)	a	s
Low-pressure absorber	2.36	−0.00372	1.58226
High-pressure absorber	6.49	−0.00534	2.22162

In the case of the tubular absorber the absorption heat is extracted by cooling water from the inside of the absorber, so solution is kept subcooled and absorption process continues after the entrance region until the end of the absorber. As result, more absorption heat is generated at the liquid–vapour interface and the vapour continues being heated (Fig. 5 from [57]). In the spray absorption process, no absorption heat is extracted. Consequently the absorption capacity of the solution is reduced, the total heat generated at the interface is smaller and, as result, the temperature increase of the vapour is also smaller. A rough estimate of the maximum error of this assumption gave values equal to 0.59% and 2.48% for the low- and high-pressure absorbers, respectively.

Finally, the next condition is to be fulfilled:

at $\theta = 0$ and $\theta = \pi$,

$$\frac{\partial x}{\partial \theta} = \frac{\partial T}{\partial \theta} = 0 \quad \text{for } t > 0 \tag{11}$$

Relative movement between the droplet and the surrounding fluid can induce circulatory motion inside the droplet and affect the mass and heat transfer. Circulatory velocity components u_r and u_θ (Fig. 3), in Eqs. (4) and (5), should be known before solving Eqs. (4)–(11). These circulatory velocities depend on the Reynolds number.

In the present study Reynolds numbers are in the range $1 \leqslant Re < 10$. The fluid recirculation and wake formation in the rear of the droplet only begin for Reynolds numbers higher that 20 according to Clift et al. [58]. Therefore the results obtained using Hadamard–Rybczynski equations for $Re < 1$ could be approximately valid. Nevertheless the cases of $Re < 1$ and $10 \leqslant Re \leqslant 250$ are analysed in the following aiming a comparison between both equations sets. Equations for calculating the circulatory velocities are given.

4.1.1. Case of $Re < 1$

In the case of fluid spheres with $Re < 1$ the stream function φ of Hadamard–Rybczynski, in spherical coordinates with the origin on the sphere centre, is given by Clift et al. [58] and Happel and Brenner [59]:

$$\varphi = \frac{u}{R^2}\left(\frac{R^2 r^2 - r^4}{4(1+\gamma)}\right)\sin^2\theta, \quad r \leqslant R$$

where u is the droplet velocity. The velocity components can be obtained through the following equations [58]:

$$u_r = -\frac{1}{r^2 \sin\theta}\frac{\partial \varphi}{\partial \theta}; \quad u_\theta = -\frac{1}{r\sin\theta}\frac{\partial \varphi}{\partial r}$$

that can be expressed as

$$u_r = -Pe^J\left(\frac{D}{R}\right)\left(1 - \left(\frac{r}{R}\right)^2\right)\cos\theta \tag{12}$$

$$u_\theta = Pe^J\left(\frac{D}{R}\right)\left(1 - 2\left(\frac{r}{R}\right)^2\right)\sin\theta \tag{13}$$

The modified Peclet number:

$$Pe^J = \frac{Pe}{4(1+\gamma)}$$

is used to correct the effects of the liquid and vapour viscosity ratio.

Radial velocity is maximum for r approaching 0 according to Eq. (12). It means that fluid accelerates as it approaches to the droplet centre. Inside the droplet there is a recirculation motion which moves solution from the droplet surface towards the droplet centre. Velocity in the droplet core must be larger than in the periphery by means of continuity arguments. In effect, due to the recirculation zone topology, $\pi P^2 u_P \sim \pi r^2 u_r$, where u_P is the velocity in a point very close to the periphery ($P \approx R$). Consequently, $u_r \sim (P/r)^2 u_P > u_P$ since $P > r$.

To simplify the calculation the following dimensionless variables are introduced:

$$\bar{x} = \frac{x}{x_0}, \quad \overline{T} = \frac{T}{T_0}, \quad \bar{r} = \frac{r}{R} \quad \tau = \frac{D \cdot t}{R^2}$$

For the case of $Re < 1$, substituting Eqs. (12) and (13) in Eqs. (4) and (5), Eqs. (4)–(11) can be rewritten as follows:

$$\frac{\partial \bar{x}}{\partial \tau} = \frac{\partial^2 \bar{x}}{\partial \bar{r}^2} + \frac{2}{\bar{r}}\frac{\partial \bar{x}}{\partial \bar{r}} + \frac{\cot\theta}{\bar{r}^2}\frac{\partial \bar{x}}{\partial \theta} + \frac{1}{\bar{r}^2}\frac{\partial^2 \bar{x}}{\partial \theta^2} + Pe^J\left((1-\bar{r}^2)\cos\theta\frac{\partial \bar{x}}{\partial \bar{r}} + \left(\frac{2\cdot\bar{r}^2 - 1}{\bar{r}}\right)\sin\theta\frac{\partial \bar{x}}{\partial \theta}\right) \tag{14}$$

$$\frac{\partial \overline{T}}{\partial \tau} = Le\left(\frac{\partial^2 \overline{T}}{\partial \bar{r}^2} + \frac{2}{\bar{r}}\frac{\partial \overline{T}}{\partial \bar{r}} + \frac{\cot\theta}{\bar{r}^2}\frac{\partial \overline{T}}{\partial \theta} + \frac{1}{\bar{r}^2}\frac{\partial^2 \overline{T}}{\partial \theta^2}\right) + Pe^J\left((1-\bar{r}^2)\cos\theta\frac{\partial \overline{T}}{\partial \bar{r}} + \left(\frac{2\cdot\bar{r}^2 - 1}{\bar{r}}\right)\sin\theta\frac{\partial \overline{T}}{\partial \theta}\right) \tag{15}$$

The initial conditions are

for $\tau = 0$,

$$\bar{x} = \overline{T} = 1 \quad \text{for all } \bar{r} \tag{16}$$

And the boundary conditions:

at $\bar{r} = 0$,

$$\frac{\partial \bar{x}}{\partial \bar{r}} = \frac{\partial \overline{T}}{\partial \bar{r}} = 0 \quad \text{for } \tau > 0 \tag{17}$$

at $\bar{r} = 1$,

$$\bar{x} = \bar{x}_{\text{eq}} \text{ and } \overline{T} = \overline{T}_{\text{eq}} \quad \text{for } \tau > 0 \tag{18}$$

and

$$\bar{x}_{eq} = \left(\frac{a \cdot T_0}{x_0}\right)\overline{T}_{eq} + \frac{s}{x_0} \tag{19}$$

$$-\frac{L \cdot D}{C_p \cdot \alpha}\left(\frac{x_0}{a \cdot T_0}\right)\frac{\partial \bar{x}}{\partial \bar{r}_{\bar{r}=1}} = \frac{\partial \overline{T}}{\partial \bar{r}_{\bar{r}=1}} \tag{20}$$

also,

at $\theta = 0$ and $\theta = \pi$,

$$\frac{\partial \bar{x}}{\partial \theta} = \frac{\partial \overline{T}}{\partial \theta} = 0 \quad \text{for } \tau > 0 \tag{21}$$

The joint solution of Eqs. (14)–(21) allows describing the mass and heat transfer processes between refrigerant vapour and solutions droplets.

4.1.2. Case of $10 \leqslant Re \leqslant 250$

Equations to describe the flow field for $Re \geqslant 10$ are found in the literature. Among these equations are those reported by Uribe-Ramírez and Korchinsky [25] for $10 \leqslant Re \leqslant 250$. The equations given for calculating the velocity components inside the droplet are the following:

$$u_r = -2[(c_1 + c_2\bar{r} + c_3\bar{r}^2)\cos\theta + (d_1 + d_2\bar{r} + d_3\bar{r}^2) \times (\cos^2\theta - \tfrac{1}{2}\sin^2\theta)] \tag{12a}$$

$$u_\theta = -[(2c_1 + 3c_2\bar{r} + 4c_3\bar{r}^2)\sin\theta + (2d_1 + 3d_2\bar{r} + 4d_3\bar{r}^2) \times \sin\theta\cos\theta] \tag{13a}$$

Constants that appear in Eqs. (12a) and (13a) are obtained through the solution of the system of equations shown in Appendix A. Using Eqs. (12a) and (13a), Eqs. (14) and (15) are transformed into the followings:

$$\begin{aligned}\frac{\partial \bar{x}}{\partial \tau} &= \frac{\partial^2 \bar{x}}{\partial \bar{r}^2} + \frac{2}{\bar{r}}\frac{\partial \bar{x}}{\partial \bar{r}} + \frac{\cot\theta}{\bar{r}^2}\frac{\partial \bar{x}}{\partial \theta} + \frac{1}{\bar{r}^2}\frac{\partial^2 \bar{x}}{\partial \theta^2} \\ &+ 2\frac{R}{D}\left[(c_1 + c_2R\bar{r} + c_3R^2\bar{r}^2)\cos\theta\right]\frac{\partial \bar{x}}{\partial \bar{r}} \\ &+ 2\frac{R}{D}\left[(d_1 + d_2R\bar{r} + d_3R^2\bar{r}^2)\left(\cos^2\theta - \frac{1}{2}\sin^2\theta\right)\right]\frac{\partial \bar{x}}{\partial \bar{r}} \\ &+ \frac{R}{D\bar{r}}\left[(2c_1 + 3c_2R\bar{r} + 4c_3R^2\bar{r}^2)\sin\theta\right. \\ &\left.+ (2d_1 + 3d_2R\bar{r} + 4d_3R^2\bar{r}^2)\sin\theta\cos\theta\right]\frac{\partial \bar{x}}{\partial \theta}\end{aligned} \tag{14a}$$

$$\begin{aligned}\frac{\partial \overline{T}}{\partial \tau} &= Le\left(\frac{\partial^2 \overline{T}}{\partial \bar{r}^2} + \frac{2}{\bar{r}}\frac{\partial \overline{T}}{\partial \bar{r}} + \frac{\cot\theta}{\bar{r}^2}\frac{\partial \overline{T}}{\partial \theta} + \frac{1}{\bar{r}^2}\frac{\partial^2 \overline{T}}{\partial \theta^2}\right) \\ &+ 2\frac{R}{D}\left[(c_1 + c_2R\bar{r} + c_3R^2\bar{r}^2)\cos\theta\right]\frac{\partial \overline{T}}{\partial \bar{r}} \\ &+ 2\frac{R}{D}\left[(d_1 + d_2R\bar{r} + d_3R^2\bar{r}^2)\left(\cos^2\theta - \frac{1}{2}\sin^2\theta\right)\right]\frac{\partial \overline{T}}{\partial \bar{r}} \\ &+ \frac{R}{D\bar{r}}\left[(2c_1 + 3c_2R\bar{r} + 4c_3R^2\bar{r}^2)\sin\theta\right. \\ &\left.+ (2d_1 + 3d_2R\bar{r} + 4d_3R^2\bar{r}^2)\sin\theta\cos\theta\right]\frac{\partial \overline{T}}{\partial \theta}\end{aligned} \tag{15a}$$

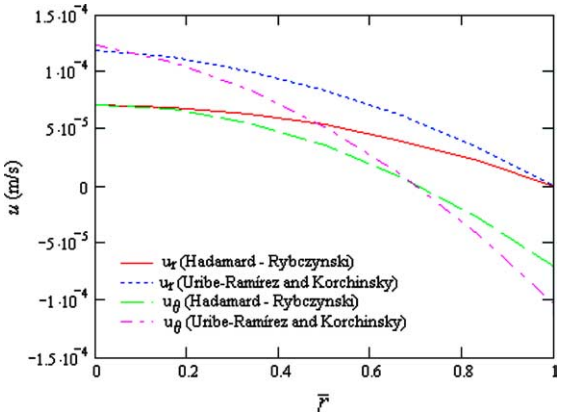

Fig. 4. Comparison of velocity profiles inside the droplet (low-pressure absorber, $\theta = 3\pi/4$).

The initial and boundary conditions (16)–(21) continue being valid.

Fig. 4 shows a comparison between radial and tangential velocity profiles inside the droplet using both equations sets. It can be observed that quite similar profiles are obtained. The small velocity of droplets is the reason of this performance.

4.2. Numerical solution of the heat and mass transfer problem

For the numerical solution of Eqs. (14) or (14a) and (15) or (15a) and the corresponding initial and boundary conditions (16)–(21) a finite difference method is used. The application of the finite difference technique to partial differential equations, as Eqs. (14), (14a) and (15), (15a), is described by Anderson et al. [60]. This technique has been extensively used to solve heat or mass transfer problems in spherical droplets and boundary layers problems [31–35,37,38,46,61]. A totally implicit method has been selected, in this case the Crank-Nicholson method due to the following reasons:

- Implicit techniques are unconditionally stable, without limitations for temporal step ($\Delta\tau$) or grid step ($\Delta\bar{r}$ and $\Delta\theta$) selection. The global precision of the discretised equations, on second order finite difference, is of order $O(\Delta\tau, \Delta\theta^2, \Delta\bar{r}^2)$.
- This technique has proved its effectiveness to solve a wide range of transport problems [13,14,32].

Eqs. (14,14a)–(21) have been discretised to obtain algebraic equations (Appendices B and C) using the computational grid shown in Fig. 5. The grid space in these algebraic equations is determined through

$$\Delta\bar{r} = \frac{1}{nr - 1}; \quad \Delta\theta = \frac{\pi}{ncita - 1}$$

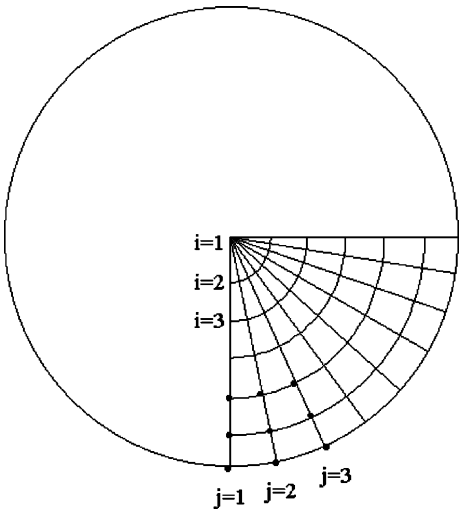

Fig. 5. Computational grid for the finite difference discretisation.

where 'nr' and 'ncita' represent the points number in r and θ directions, respectively.

In the algebraic equations that appear in Appendix B, for $Re < 1$ and $10 \leqslant Re \leqslant 250$, n represents the iteration number. Initial and boundary conditions are given in Appendix C for both cases.

The system of algebraic equations obtained can be represented in vectorial form as

$$C \cdot l^{n+1} = W \cdot l^{n} \tag{22}$$

where vectors C, W and l take the form shown in Appendix D. Subscript LL in matrices C and W of Appendix D corresponds to the dimension of the $2 \cdot \mathrm{nr} \cdot \mathrm{ncita}$ matrix used to store the solution of the two time levels used in the finite difference scheme. Coefficients a_{ij} are obtained from Eqs. (B.1)–(B.4), (C.1)–(C.6) of Appendices B and C. The solution of this system of equations gives the ammonia concentration and temperature in each time instant for each point inside the droplet. To solve the equation system (22) a numerical program in MATLAB 5.3 code [62] has been developed.

5. Simulation results

5.1. Low-pressure absorber

The following data, previously described for the low-pressure absorber, have been considered in the simulation:

- Droplets of 60 μm diameter fall at their terminal velocity corresponding to 0.17 m/s.
- Selected data correspond to a typical example of a double-stage absorption refrigeration cycle. The case when the refrigerant vapour is separated at 85 °C is selected. Solution and vapour properties appear in Tables 1 and 2.

Fig. 6 shows the three-dimensional radial and time evolution of ammonia concentration at the droplet frontal position ($\theta = 0$, Fig. 3) using Hadamard–Rybczynski equations. In this case a solution subcooling of 14 °C has been considered.

It can be observed that the droplet achieves the equilibrium state in a dimensionless time approximately equal to 0.5, which corresponds to 0.61 s for the reference conditions. The time obtained to achieve equilibrium is very short. It implies that the absorber length also will be small. Considering the droplets terminal velocity, when they have travelled approximately 10 cm they have already achieved the equilibrium state. Final droplet concentration is equal to 38.6% of ammonia and temperature is 321.5 K.

The influence of subcooling is considerable in the droplets final concentration. Evolution of droplet concentration is shown in Fig. 7 for similar conditions to Fig. 6, except with 19 °C subcooling. For these new conditions the final ammonia concentration is higher, 39.2%, and the temperature is 320 K. Table 4 summarises these results.

Increase of subcooling makes that droplets absorb more refrigerant vapour and consequently they heat more. This result is important when designing spray absorbers because less solution recirculation will be necessary. Also, less pump power and solution amount may be required in the absorption machine.

Global results obtained in the simulation using the equations given by Uribe-Ramírez and Korchinsky [25] coincide with those of Hadamard–Rybczynski. When

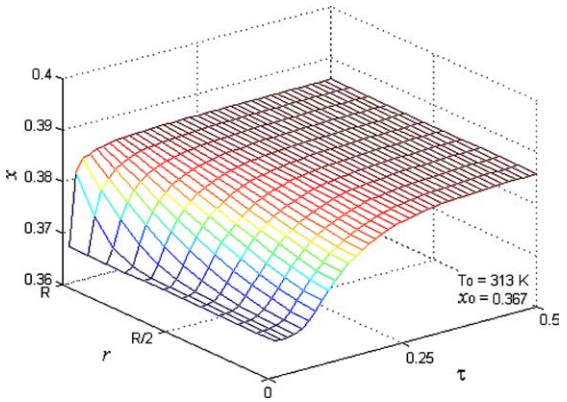

Fig. 6. Radial and time evolution of droplet ammonia concentration ($T_0 = 313$ K, low-pressure absorber, subcooling = 14 °C).

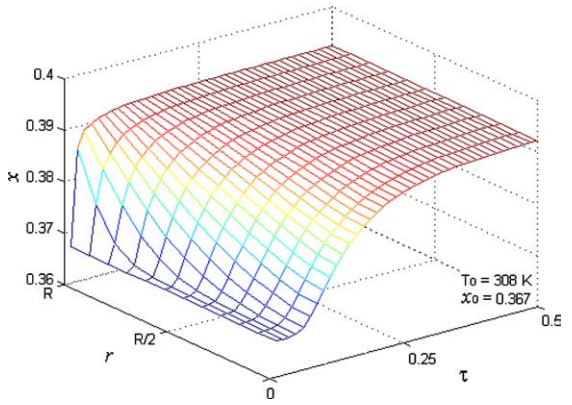

Fig. 7. Radial and time evolution of droplet ammonia concentration ($T_0 = 308$ K, low-pressure absorber, subcooling = 19 °C).

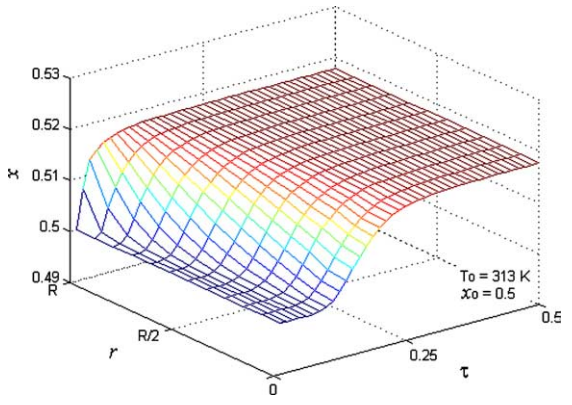

Fig. 8. Radial and time evolution of droplet ammonia concentration ($T_0 = 313$ K, high-pressure absorber, subcooling = 10 °C).

Table 4
Effect of subcooling in the low-pressure absorber

x_0 (%)	T_0 (K)	Subcooling (K)	x (%)	Δx (%)	T (K)	ΔT (K)
36.7	313	14	38.6	1.9	321.5	8.5
36.7	308	19	39.2	2.5	320	12

equations given by Uribe-Ramírez and Korchinsky are used the droplets also achieve the equilibrium state in a dimensionless time equal to 0.5. The reason for obtaining similar results could be the similarity shown in Fig. 4 between both velocity profiles inside the droplets. Nextly, it will be shown that, in spite of achieving the equilibrium in a similar time, the time evolution of concentration does not exactly have the same behaviour using both sets of equations. The fact that these equations have been developed for different flow regimens could be a reason for the difference.

5.2. High-pressure absorber

The following data, previously described for the high-pressure absorber, have been considered:

- Droplets of 100 μm diameter fall at their terminal velocity corresponding to 0.29 m/s.
- Selected data also correspond to the example of the double-stage absorption refrigeration cycle when refrigerant vapour is separated at 85 °C. Solution and vapour properties are given in Tables 1 and 2.

In this case, trends obtained coincide with those for the low-pressure absorber. In Figs. 8 and 9 the time and radial evolution of ammonia concentration in the front of the droplets appears, for subcooling equal to 10 and 15 °C, respectively. It can be observed that the degree of

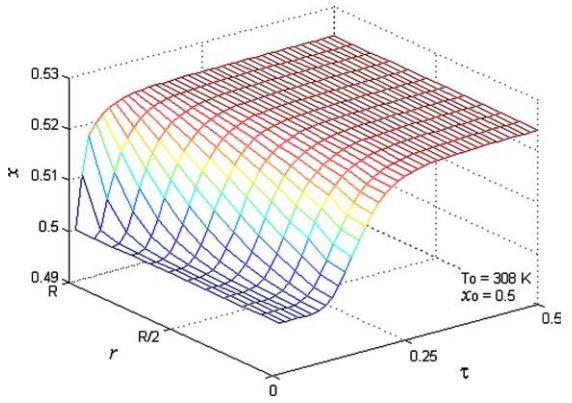

Fig. 9. Radial and time evolution of droplet ammonia concentration ($T_0 = 308$ K, high-pressure absorber, subcooling = 15 °C).

subcooling is different in both absorbers. It was selected considering two cases for the solution temperature at the outlet of the solution heat exchangers: 35 and 40 °C. These temperatures are considered to be similar in both absorbers because similar heat exchangers, flows and temperature differences are used. Taking into account the pressure existing in both absorption chambers (Table 3), these temperatures translate into different solution subcooling for the low (high) pressure absorber.

Similar to the low-pressure absorber, the time required to achieve equilibrium is very short. It is equal to 0.5 in dimensionless time and corresponds to 0.77 s for the case considered. It implies that the absorber length also will be very small. Considering the droplets terminal velocity inside the absorber, they achieve equilibrium when they have travelled 23 cm approximately.

In this case a higher subcooling also yields an increase in the amount of refrigerant vapour absorbed. Thus, the final ammonia concentration of droplets will

Table 5
Effect of subcooling in the high-pressure absorber

x_0 (%)	T_0 (K)	Subcooling (K)	x (%)	Δx (%)	T (K)	ΔT (K)
50	313	10	51.8	1.8	319	6
50	308	15	52.4	2.4	318	10

be higher. When subcooling is equal to 10 °C the droplets achieve an ammonia concentration equal to 51.8% and a temperature equal to 319 K. When the subcooling corresponds to 15 °C the final ammonia concentration is 52.4% and the temperature is 318 K. Results correspond to a time equal to 0.77 s in both cases. Table 5 summarises these results.

Similar to the low-pressure absorber the global results obtained in the simulation using the equations given by Uribe-Ramírez and Korchinsky [25] coincide with those obtained using Hadamard–Rybczynski equations. Droplets achieve the equilibrium in a dimensionless time equal to 0.5 in both cases.

In the present study the uniform movement of droplets inside the absorption chambers has been used for showing the results of the heat and mass transfer model. This simulation model is used in [63,64] to design the low-pressure absorber of the lithium nitrate–ammonia refrigeration system considered in the present case. In these studies all regions of the atomisation process are analysed. It is shown that 20 cm of absorption chamber length are required to achieve the equilibrium state. In a similar way the simulation procedure may be also used to study the absorption processes using the ammonia–water and lithium bromide–water solutions.

In the following section simulation results are compared with those obtained using Newman model for mass transfer [17]. For the comparison the factor E, defined as the dimensionless approach of the droplet to the equilibrium state during its lifetime (x/x_{eq}), is used. E takes 1 as the maximum value. This value indicates that the droplet has reached the equilibrium state.

6. Comparison with Newman model

The present study is the first application of Newman model to refrigeration absorption systems using the lithium nitrate–ammonia solution. Ryan [4] employs this model for the case of the lithium bromide–water solution to evaluate the absorption of water vapour by droplets of 200 μm diameter moving at different velocities.

Fig. 10 shows the evolution of E with time according to:

- Newman model.
- Results of the present study.

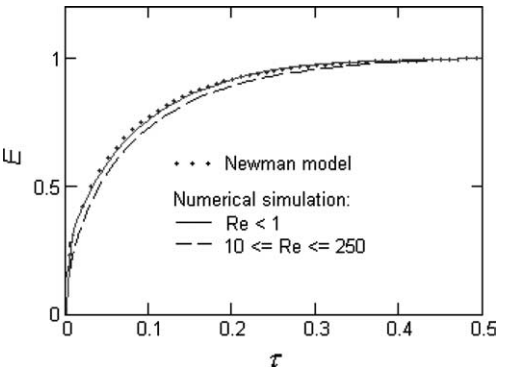

Fig. 10. Dimensionless evolution of absorption process.

Graphically it can be observed that droplets achieve the equilibrium state in a dimensionless time equal to 0.5 using Newman model. This value coincides with the numerical simulation results. It can be observed that simulation results obtained using the equations given by Uribe-Ramírez and Korchinsky [25] coincide with those of Hadamard–Rybczynski, regarding to the dimensionless time required to achieve equilibrium. Time evolution of concentration does not follow exactly the same patron with both sets of equations. The fact that these equations have been developed for different flow regimes could be the reason for this difference.

Newman model was experimentally validated by Ryan et al. [5] for lithium bromide–water droplets of diameters ranging from 200 to 500 μm. The authors obtain deviations in the results, respect to the model prediction, included in the error range of the experimental equipment. According to the authors the model predicts with a precision equal to 98%.

In the present case results are also similar to the prediction of Newman model because very fine droplets have been used. These droplets behave like rigid and their internal circulation is insignificant. Newman model considers the droplet rigid; that is, molecular diffusion is the only responsible for solute absorption. In the present study the speed of absorption reaches values of the order of 6×10^{-4} m/s, while maximum values of the speed of circulation are about five times lower (Fig. 4). The case of zero velocity was not considered in the present study because it does not represent a real case inside a spray absorption chamber. If it were considered results obtained would have a better approach to Newman model results.

Then, it can be concluded that Newman model is valid to evaluate the mass transfer to very small lithium nitrate–ammonia droplets. This model may be applied, given the initial conditions, with a simple overall balance of what the equilibrium state would be. It also may be used for estimating the required time to achieve the equilibrium state. However, this model does not allow

determining the concentration profiles inside droplets. The numerical procedure developed is required in this case.

7. Conclusions

In the present study a model for the simultaneous heat and mass transfer in droplets has been developed. This model allows prediction of the absorption of refrigerant vapour by dispersed droplets in adiabatic spray absorbers. The following conclusions were drawn:

- Simulation permits obtaining the concentration profiles inside the lithium nitrate–ammonia droplets as a function of the time. Solution droplets reach the equilibrium state in a dimensionless time equal to 0.5 that corresponds to times smaller than 1 s. Consequently, absorbers length may be very small.
- Increase of subcooling makes that droplets absorb more refrigerant vapour. Then, less solution recirculation, pump power and solution mass may be necessary in the absorption machine.
- Newman model is adequate for predicting mass transfer to the droplets analysed of 60 and 100 μm diameter, because the internal circulation is insignificant and droplets behave like rigid. Molecular diffusion dominates the mass transfer process. This model may be also used for estimating the time required to reach the equilibrium state. However, the numerical procedure developed is necessary to determine the concentration profiles inside the droplets.
- The procedure developed and the results obtained from the simulation may be used for designing spray absorbers of absorption refrigeration systems using the lithium nitrate–ammonia pair. The usefulness of the simulation procedure extends to others solutions.

Acknowledgements

The authors wish to express their gratitude to the Ministerio de Ciencia y Tecnología for the financial support of this research through the projects DPI2002-02439. Also, M. Venegas wishes to thank to the Agencia Española de Cooperación Internacional for the PhD fellowship granted.

Appendix A

$$a_1 + a_2 + a_3 = -1/2$$

$$b_1 + b_2 + b_3 = 0$$

$$c_1 + c_2 + c_3 = 0$$

$$d_1 + d_2 + d_3 = 0$$

$$a_1 + 2a_2 + 3a_3 = 1 - 2c_1 - 3c_2 - 4c_3$$

$$b_1 + 2b_2 + 3b_3 = -2d_1 - 3d_2 - 4d_3$$

$$3a_1 + 6a_2 + 10a_3 = \gamma(c_2 + 3c_3)$$

$$5b_1 + 8b_2 + 12b_3 = \gamma(2d_1 + 3d_2 + 5d_3)$$

$$\left(8c_1d_1 + 5c_2d_2 + \frac{20}{3}c_3d_1 - 6c_1d_3 - \frac{4}{3}c_2d_2 - \frac{36}{5}c_3d_3 - \frac{31}{4}c_3d_2\right)Re_d + 14c_2 = 0$$

$$\left(2c_1c_2 + \frac{3}{2}c_2^2 + \frac{1}{2}d_1d_3 - \frac{9}{5}d_2d_3 + \frac{6}{5}c_2c_3 - 2d_3^2 + 2d_1^2 + 2d_1d_2\right)Re_d - 18d_1 + 6d_3 = 0$$

$$\left(12a_2b_3 - 46a_2b_1 - \frac{784}{9}a_3b_1 - \frac{64}{3}a_2b_2 + \frac{80}{3}a_1b_3 - 56a_3b_2 - 16a_3b_3 - \frac{128}{7}a_1b_1\right)Re_c + (2b_3 + 2b_1)Re_c - 56(3a_2 + 10a_3) = 0$$

$$\left(\frac{94}{11}a_2a_3 + \frac{4}{11}b_2b_3 - \frac{1}{5}b_1b_3 + \frac{8}{3}a_1a_2 - \frac{8}{27}b_1b_2 + \frac{1}{2}b_3^2 - \frac{1}{6}b_1^2 + \frac{12}{5}a_2^2 + 2a_2\right)Re_c + \left(5a_3 + \frac{35}{6}a_3^2 + 7a_1a_3\right)Re_c + 2b_1 - 9b_3 = 0$$

Appendix B

Case of $Re < 1$

Mass transfer:

$$\frac{\bar{x}_{i,j}^{n+1} - \bar{x}_{i,j}^{n}}{\Delta\tau} = \frac{\bar{x}_{i+1,j}^{n+1} - 2\bar{x}_{i,j}^{n+1} + \bar{x}_{i-1,j}^{n+1}}{2\Delta\bar{r}^2} + \frac{\bar{x}_{i+1,j}^{n} - 2\bar{x}_{i,j}^{n} + \bar{x}_{i-1,j}^{n}}{2\Delta\bar{r}^2} + \frac{\bar{x}_{i,j+1}^{n+1} - 2\bar{x}_{i,j}^{n+1} + \bar{x}_{i,j-1}^{n+1}}{2\bar{r}_i^2\Delta\theta^2} + \frac{\bar{x}_{i,j+1}^{n} - 2\bar{x}_{i,j}^{n} + \bar{x}_{i,j-1}^{n}}{2\bar{r}_i^2\Delta\theta^2} + \left(\frac{2}{\bar{r}_i} + Pe^J(1 - \bar{r}_i^2)\cos\theta_j\right)\frac{\bar{x}_{i+1,j}^{n+1} - \bar{x}_{i-1,j}^{n+1} + \bar{x}_{i+1,j}^{n} - \bar{x}_{i-1,j}^{n}}{4\Delta\bar{r}} + \left(\frac{\cot\theta_j}{\bar{r}_i^2} + Pe^J\left(\frac{2\bar{r}_i^2 - 1}{\bar{r}_i}\right)\sin\theta_j\right) \times \frac{\bar{x}_{i,j+1}^{n+1} - \bar{x}_{i,j-1}^{n+1} + \bar{x}_{i,j+1}^{n} - \bar{x}_{i,j-1}^{n}}{4\Delta\theta} \quad \text{(B.1)}$$

Heat transfer:

$$\begin{aligned}
&\frac{\overline{T}_{i,j}^{n+1}-\overline{T}_{i,j}^{n}}{\Delta\tau}\\
&\quad=Le\frac{\overline{T}_{i+1,j}^{n+1}-2\overline{T}_{i,j}^{n+1}+\overline{T}_{i-1,j}^{n+1}}{2\Delta\bar{r}^2}\\
&\qquad+Le\frac{\overline{T}_{i+1,j}^{n}-2\overline{T}_{i,j}^{n}+\overline{T}_{i-1,j}^{n}}{2\Delta\bar{r}^2}\\
&\qquad+Le\frac{\overline{T}_{i,j+1}^{n+1}-2\overline{T}_{i,j}^{n+1}+\overline{T}_{i,j-1}^{n+1}}{2\bar{r}_i^2\Delta\theta^2}\\
&\qquad+Le\frac{\overline{T}_{i,j+1}^{n}-2\overline{T}_{i,j}^{n}+\overline{T}_{i,j-1}^{n}}{2\bar{r}_i^2\Delta\theta^2}\\
&\qquad+\left(\frac{2\cdot Le}{\bar{r}_i}+Pe^{J}(1-\bar{r}_i^2)\cos\theta_j\right)\\
&\qquad\times\frac{\overline{T}_{i+1,j}^{n+1}-\overline{T}_{i-1,j}^{n+1}+\overline{T}_{i+1,j}^{n}-\overline{T}_{i-1,j}^{n}}{4\Delta\bar{r}}\\
&\qquad+\left(\frac{\cot\theta_j Le}{\bar{r}_i^2}+Pe^{J}\left(\frac{2\bar{r}_i^2-1}{\bar{r}_i}\right)\sin\theta_j\right)\\
&\qquad\times\frac{\overline{T}_{i,j+1}^{n+1}-\overline{T}_{i,j-1}^{n+1}+\overline{T}_{i,j+1}^{n}-\overline{T}_{i,j-1}^{n}}{4\Delta\theta}
\end{aligned}\tag{B.2}$$

Case of $10\leqslant Re\leqslant 250$

Mass transfer:

$$\begin{aligned}
&\frac{\bar{x}_{i,j}^{n+1}-\bar{x}_{i,j}^{n}}{\Delta\tau}\\
&\quad=\frac{\bar{x}_{i+1,j}^{n+1}-2\bar{x}_{i,j}^{n+1}+\bar{x}_{i-1,j}^{n+1}}{2\Delta\bar{r}^2}+\frac{\bar{x}_{i+1,j}^{n}-2\bar{x}_{i,j}^{n}+\bar{x}_{i-1,j}^{n}}{2\Delta\bar{r}^2}\\
&\qquad+\frac{\bar{x}_{i,j+1}^{n+1}-2\bar{x}_{i,j}^{n+1}+\bar{x}_{i,j-1}^{n+1}}{2\bar{r}_i^2\Delta\theta^2}+\frac{\bar{x}_{i,j+1}^{n}-2\bar{x}_{i,j}^{n}+\bar{x}_{i,j-1}^{n}}{2\bar{r}_i^2\Delta\theta^2}\\
&\qquad+\left(\frac{2}{\bar{r}_i}+2\frac{R}{D}[(c_1+c_2R\bar{r}_i+c_3R^2\bar{r}_i^2)\cos\theta_j]\right)\\
&\qquad\times\frac{\bar{x}_{i+1,j}^{n+1}-\bar{x}_{i-1,j}^{n+1}+\bar{x}_{i+1,j}^{n}-\bar{x}_{i-1,j}^{n}}{4\Delta\bar{r}}\\
&\qquad+\frac{2R}{D}\left[(d_1+d_2R\bar{r}_i+d_3R^2\bar{r}_i^2)\left(\cos^2\theta_j-\frac{\sin^2\theta_j}{2}\right)\right]\\
&\qquad\times\frac{\bar{x}_{i+1,j}^{n+1}-\bar{x}_{i-1,j}^{n+1}+\bar{x}_{i+1,j}^{n}-\bar{x}_{i-1,j}^{n}}{4\Delta\bar{r}}\\
&\qquad+\left(\frac{\cot\theta_j}{\bar{r}_i^2}\right)\frac{\bar{x}_{i,j+1}^{n+1}-\bar{x}_{i,j-1}^{n+1}+\bar{x}_{i,j+1}^{n}-\bar{x}_{i,j-1}^{n}}{4\Delta\theta}\\
&\qquad+\left(\frac{R}{D\bar{r}_i}\left[(2c_1+3c_2R\bar{r}_i+4c_3R^2\bar{r}_i^2)\sin\theta_j\right]\right)\\
&\qquad\times\frac{\bar{x}x_{i,j+1}^{n+1}-\bar{x}_{i,j-1}^{n+1}+\bar{x}_{i,j+1}^{n}-\bar{x}_{i,j-1}^{n}}{4\Delta\theta}\\
&\qquad+\left(\frac{R}{D\bar{r}_i}\left[(2d_1+3d_2R\bar{r}_i+4d_3R^2\bar{r}_i^2)\sin\theta_j\cos\theta_j\right]\right)\\
&\qquad\times\frac{\bar{x}_{i,j+1}^{n+1}-\bar{x}_{i,j-1}^{n+1}+\bar{x}_{i,j+1}^{n}-\bar{x}_{i,j-1}^{n}}{4\Delta\theta}
\end{aligned}\tag{B.3}$$

Heat transfer:

$$\begin{aligned}
&\frac{\overline{T}_{i,j}^{n+1}-\overline{T}_{i,j}^{n}}{\Delta\tau}\\
&\quad=Le\frac{\overline{T}_{i+1,j}^{n+1}-2\overline{T}_{i,j}^{n+1}+\overline{T}_{i-1,j}^{n+1}}{2\Delta\bar{r}^2}\\
&\qquad+Le\frac{\overline{T}_{i+1,j}^{n}-2\overline{T}_{i,j}^{n}+\overline{T}_{i-1,j}^{n}}{2\Delta\bar{r}^2}\\
&\qquad+Le\frac{\overline{T}_{i,j+1}^{n+1}-2\overline{T}_{i,j}^{n+1}+\overline{T}_{i,j-1}^{n+1}}{2\bar{r}_i^2\Delta\theta^2}\\
&\qquad+Le\frac{\overline{T}_{i,j+1}^{n}-2\overline{T}_{i,j}^{n}+\overline{T}_{i,j-1}^{n}}{2\bar{r}_i^2\Delta\theta^2}\\
&\qquad+\left(\frac{2\cdot Le}{\bar{r}_i}+2\frac{R}{D}[(c_1+c_2R\bar{r}_i+c_3R^2\bar{r}_i^2)\cos\theta_j]\right)\\
&\qquad\times\frac{\overline{T}_{i+1,j}^{n+1}-\overline{T}_{i-1,j}^{n+1}+\overline{T}_{i+1,j}^{n}-\overline{T}_{i-1,j}^{n}}{4\Delta\bar{r}}\\
&\qquad+\frac{2R}{D}\left[(d_1+d_2R\bar{r}_i+d_3R^2\bar{r}_i^2)\right.\\
&\qquad\left.\times\left(\cos^2\theta_j-\frac{\sin^2\theta_j}{2}\right)\right]\frac{\overline{T}_{i+1,j}^{n+1}-\overline{T}_{i-1,j}^{n+1}+\overline{T}_{i+1,j}^{n}-\overline{T}_{i-1,j}^{n}}{4\Delta\bar{r}}\\
&\qquad+\left(\frac{\cot\theta_j Le}{\bar{r}_i^2}\right)\frac{\overline{T}_{i,j+1}^{n+1}-\overline{T}_{i,j-1}^{n+1}+\overline{T}_{i,j+1}^{n}-\overline{T}_{i,j-1}^{n}}{4\Delta\theta}\\
&\qquad+\left(\frac{R}{D\bar{r}_i}[(2c_1+3c_2R\bar{r}_i+4c_3R^2\bar{r}_i^2)\sin\theta_j]\right)\\
&\qquad\times\frac{\overline{T}_{i,j+1}^{n+1}-\overline{T}_{i,j-1}^{n+1}+\overline{T}_{i,j+1}^{n}-\overline{T}_{i,j-1}^{n}}{4\Delta\theta}\\
&\qquad+\left(\frac{R}{D\bar{r}_i}[(2d_1+3d_2R\bar{r}_i+4d_3R^2\bar{r}_i^2)\sin\theta_j\cos\theta_j]\right)\\
&\qquad\times\frac{\overline{T}_{i,j+1}^{n+1}-\overline{T}_{i,j-1}^{n+1}+\overline{T}_{i,j+1}^{n}-\overline{T}_{i,j-1}^{n}}{4\Delta\theta}
\end{aligned}\tag{B.4}$$

Appendix C

Initial conditions:

$$\bar{x}_{i,j}^{1}=\overline{T}_{i\cdot j}^{1}=1\tag{C.1}$$

Boundary conditions ($\bar{r}=0$):

$$\frac{-3\bar{x}_{1,j}^{n}+4\bar{x}_{2,j}^{n}-\bar{x}_{3,j}^{n}}{\Delta\bar{r}^2}=0;\quad\frac{-3\overline{T}_{1,j}^{n}+4\overline{T}_{2,j}^{n}-\overline{T}_{3,j}^{n}}{\Delta\bar{r}^2}=0\tag{C.2}$$

Boundary conditions ($\bar{r}=1$):

$$\bar{x}_{\bar{r}=1,j}^{n}=\frac{a\cdot T_0}{x_0}\overline{T}_{\bar{r}=1,j}^{n}+\frac{b}{x_0}\tag{C.3}$$

$$\begin{aligned}
&-\frac{L}{C_{\mathrm{p}}}\frac{D}{\alpha}\frac{C_0}{a\cdot T_0}\frac{C_{\mathrm{nr}-2,j}^{n}-4C_{\mathrm{nr}-1,j}^{n}+3C_{\mathrm{nr},j}^{n}}{\Delta r^2}\\
&\quad=\frac{T_{\mathrm{nr}-2,j}^{n}-4T_{\mathrm{nr}-1,j}^{n}+3T_{\mathrm{nr},j}^{n}}{\Delta r^2}
\end{aligned}\tag{C.4}$$

Boundary conditions ($\theta = 0$):

$$\frac{-3\bar{x}^n_{i,1} + 4\bar{x}^n_{i,2} - \bar{x}^n_{i,3}}{\Delta\theta^2} = 0; \quad \frac{-3\overline{T}^n_{i,1} + 4\overline{T}^n_{i,2} - \overline{T}^n_{i,3}}{\Delta\theta^2} = 0 \tag{C.5}$$

Boundary conditions ($\theta = \pi$):

$$\frac{\bar{x}^n_{i,\mathrm{ncita}-2} - 4\bar{x}^n_{i,\mathrm{ncita}-1} + 3\bar{x}^n_{i,\mathrm{ncita}}}{\Delta\theta^2} = 0;$$
$$\frac{\overline{T}^n_{i,\mathrm{ncita}-2} - 4\overline{T}^n_{i,\mathrm{ncita}-1} + 3\overline{T}^n_{i,\mathrm{ncita}}}{\Delta\theta^2} = 0 \tag{C.6}$$

Appendix D

$$l^{n+1} = \begin{pmatrix} \bar{x}^{n+1}_{1,1} \\ \vdots \\ \bar{x}^{n+1}_{\mathrm{nr},1} \\ \vdots \\ \bar{x}^{n+1}_{1,\mathrm{ncita}} \\ \vdots \\ \bar{x}^{n+1}_{\mathrm{nr},\mathrm{ncita}} \\ \overline{T}^{n+1}_{1,1} \\ \vdots \\ \overline{T}^{n+1}_{\mathrm{nr},1} \\ \vdots \\ \overline{T}^{n+1}_{1,\mathrm{ncita}} \\ \vdots \\ \overline{T}^{n+1}_{\mathrm{nr},\mathrm{ncita}} \end{pmatrix}$$

$$C, W = \begin{pmatrix} a_{11} & a_{12} & a_{13} & \cdots & a_{1,\mathrm{nr}+1} & & & & \mathbf{0} \\ a_{21} & a_{22} & \ddots & \ddots & \cdots & a_{2,\mathrm{nr}+1} & & & \\ a_{31} & \ddots & \ddots & \ddots & \ddots & \cdots & \ddots & & \\ \cdots & \ddots & \ddots & \ddots & \ddots & \ddots & \cdots & \ddots & \\ a_{\mathrm{nr}+1,1} & \cdots & \ddots & \ddots & \ddots & \ddots & \ddots & \cdots & \ddots \\ & a_{\mathrm{nr}+2,2} & \cdots & \ddots & \ddots & \ddots & \ddots & \ddots & \cdots & * \\ & & \ddots & \cdots & \ddots & \ddots & \ddots & \ddots & \ddots & \vdots \\ & & & \ddots & \cdots & \ddots & \ddots & \ddots & \ddots & * \\ & & & & \ddots & \cdots & \ddots & \ddots & \ddots & * \\ \mathbf{0} & & & & & * & \cdots & * & * & a_{LL} \end{pmatrix}$$

References

[1] G.A. Paniev, Absorption heat and mass transfer on droplets in a polydispersed spray, Heat Transfer—Soviet Res. 15 (5) (1983) 62–72.

[2] A.P. Burdukov, A.R. Dorokhov, G.A. Paniev, Combined heat and mass transfer in absorption on droplets, Soviet J. Appl. Phys. 3 (1) (1989) 39–45.

[3] I. Morioka, M. Kiyota, A. Ousaka, T. Kobayashi, Analysis of steam absorption by a subcooled droplet of aqueous solution of LiBr, JSME Int. J. II 35 (3) (1992) 458–464.

[4] W.A. Ryan, Water absorption in an adiabatic spray of aqueous lithium bromide solution, in: Proceedings of the International Absorption Heat Pump Conference, AES-vol. 31, ASME, 1994, pp. 155–162.

[5] W.A. Ryan, F. Ruiz, J. Wurm, Model development and verification of spray absorption for gas driven cooling systems, in: Proceedings of the International Gas Research Conference, Cannes, 1995, pp. 1483–1493.

[6] F. Summerer, P. Riesch, F. Ziegler, G. Alefeld, Hydroxide absorption heat pumps with spray absorber, ASHRAE Tech. Data Bull. 12 (1) (1996) 50–57.

[7] M. Flamensbeck, F. Summerer, P. Riesch, F. Ziegler, G. Alefeld, A cost effective absorption chiller with plate heat exchangers using water and hydroxides, Appl. Thermal Eng. 18 (6) (1998) 413–425.

[8] M. Venegas, Mass and heat transfer in droplets in lithium nitrate–ammonia absorption processes: new technologies, PhD thesis, Carlos III University of Madrid, Spain, 2002 (in Spanish).

[9] C. Keizer, Absorption refrigeration machines, PhD thesis, Delft University of Technology, Holland, 1982.

[10] C.A. Infante Ferreira, Vertical tubular absorbers for ammonia-salt absorption refrigeration, PhD thesis, Delft Technical University, Holland, 1985.

[11] T. Merrill, T. Setoguchi, H. Perez-Blanco, Compact bubble absorber design and analysis, in: Proceedings of the International Absorption Heat Pump Conference, AES-vol. 31, ASME, 1994, pp. 217–223.

[12] G.S. Herbine, H. Perez-Blanco, Model of an ammonia–water bubble absorber, ASHRAE Trans. 101 (1) (1995) 1324–1332.

[13] T. Merrill, H. Perez-Blanco, Combined heat and mass transfer during bubble absorption in binary solutions, Int. J. Heat Mass Transfer 40 (3) (1997) 589–603.
[14] T. Merrill, Thermally controlled bubble collapse in binary solutions, Int. J. Heat Mass Transfer 43 (18) (2000) 3287–3298.
[15] J. Cao, R.N. Christensen, Non-spherical bubble collapse mechanics in binary solutions, Int. J. Heat Mass Transfer 44 (2001) 1411–1423.
[16] Y.T. Kang, T. Nagano, T. Kashiwagi, Visualization of bubble behavior and bubble diameter correlation for NH_3–H_2O bubble absorption, Int. J. Refrigerat. 25 (2002) 127–135.
[17] A. Newman, The drying of porous solids: diffusion and surface emission equations, Trans. AIChE 27 (1931) 203–220.
[18] R. Kronig, J.C. Brink, On the theory of extraction from falling droplets, Appl. Sci. Res. A 2 (1950) 142–154.
[19] A. Handlos, T. Baron, Mass and heat transfer from droplets in liquid–liquid extraction, AIChE J. 3 (1957) 127–136.
[20] A.C. Lochiel, P.H. Calderbank, Mass transfer in the continuous phase around axisymmetric bodies of revolution, Chem. Eng. Sci. 19 (1964) 471–484.
[21] P.M. Rose, R.C. Kintner, Mass transfer from large oscillating droplets, AIChE J. 12 (3) (1966) 530–534.
[22] E. Ruckenstein, Mass transfer between a single drop and a continuous phase, Int. J. Heat Mass Transfer 10 (1967) 1785–1792.
[23] B.T. Chao, Transient heat and mass transfer to a translating droplet, J. Heat Transfer, Trans. ASME 91 (1969) 273–281.
[24] E. Ruckenstein, Prediction of rates of heat or mass transfer in complex situations by interpolating between simpler limiting cases, Chem. Eng. Sci. 37 (1982) 1505–1511.
[25] A.R. Uribe-Ramírez, W.J. Korchinsky, Fundamental theory for prediction of single-component mass transfer in liquid droplets at intermediate Reynolds numbers ($10 \leqslant Re \leqslant 250$), Chem. Eng. Sci. 55 (2000) 3305–3318.
[26] D. Herskowits, V. Herskowits, K. Stephan, A. Tamir, Characterization of a two-phase impinging jet absorber—I. Physical absorption of CO_2 in water, Chem. Eng. Sci. 43 (1988) 2773–2780.
[27] M.H. Oyevaar, R. Nos, K.R. Westerterp, Interfacial areas and gas hold-ups in gas–liquid contactors at elevated pressures from 0.1 to 8.0 MPa, Chem. Eng. Sci. 46 (1991) 1217–1231.
[28] A. Dimiccoli, M. Di Serio, E. Santacesaria, Mass transfer and kinetics in spray-tower-loop absorbers and reactors, Ind. Eng. Chem. Res. 39 (2000) 4082–4093.
[29] R.V. Shilimkan, J.B. Stepanek, Mass transfer in cocurrent gas–liquid flow: gas side mass transfer coefficients in upflow, interfacial areas and mass transfer coefficient in gas and liquid in downflow, Chem. Eng. Sci. 33 (1978) 1675–1680.
[30] J.J.C. Cruz-Pinto, W.J. Korchinsky, Exact solutions of the Newman, and of the Handlos-Baron, model equations for countercurrent flow extraction, Comput. Chem. Eng. 7 (1983) 19–25.
[31] J.N. Chung, P.S. Ayyaswamy, S.S. Sadhal, Laminar condensation on a moving drop. Part 2. Numerical solutions, J. Fluid Mech. 139 (1984) 131–144.
[32] T. Sundararajan, P.S. Ayyaswamy, Numerical evaluation of heat and mass transfer to a moving liquid drop experiencing condensation, Numer. Heat Transfer 8 (1985) 689–706.
[33] D.W.F. Brilman, W.P.M. van Swaaij, G.F. Versteeg, A one-dimensional instationary heterogeneous mass transfer model for gas absorption in multiphase systems, Chem. Eng. Process. 37 (1998) 471–488.
[34] C. Lin, M. Zhou, C.J. Xu, Axisymmetrical two-dimensional heterogeneous mass transfer model for the absorption of gas into liquid–liquid dispersions, Chem. Eng. Sci. 54 (1999) 389–399.
[35] D.W.F. Brilman, M.J.V. Goldschmidt, G.F. Versteeg, W.P.M. van Swaaij, Heterogeneous mass transfer models for gas absorption in multiphase systems, Chem. Eng. Sci. 55 (2000) 2793–2812.
[36] Z.S. Mao, T. Li, J. Chen, Numerical simulation of steady and transient mass transfer to a single drop dominated by external resistance, Int. J. Heat Mass Transfer 44 (2001) 1235–1247.
[37] Gh. Juncu, Unsteady heat and/or mass transfer from a fluid sphere in creeping flow, Int. J. Heat Mass Transfer 44 (2001) 2239–2246.
[38] Z.G. Feng, E.E. Michaelides, Heat and mass transfer coefficients of viscous spheres, Int. J. Heat Mass Transfer 44 (2001) 4445–4454.
[39] W.H. Chen, Dynamics of sulfur dioxide absorption in a raindrop falling at terminal velocity, Atmos. Environ. 35 (2001) 4777–4790.
[40] W.H. Chen, Unsteady absorption of sulfur dioxide by an atmospheric water droplet with internal circulation, Atmos. Environ. 35 (2001) 2375–2393.
[41] T. Vesala, A.U. Hannemann, B.P. Luo, M. Kulmala, Th. Peter, Rigorous treatment of time-dependent trace gas uptake by droplets including bulk diffusion and surface accommodations, J. Aerosol Sci. 32 (2001) 843–860.
[42] Ch. Brogren, H.T. Karlsson, Modeling the absorption of SO_2 in a spray scrubber using the penetration theory, Chem. Eng. Sci. 52 (1997) 3085–3099.
[43] J.F. Widmann, E.J. Davis, Analysis of mass transfer between a sequence of droplets and a surrounding gas, J. Aerosol Sci. 28 (1997) 1233–1249.
[44] V.E. Nakoryakov, N.I. Grigoreva, Combined heat and mass transfer during absorption in droplets and films, J. Eng. Phys. 32 (3) (1977) 243–247.
[45] D.L. Fenton, A.F. Noeth, R.L. Gorton, Absorption of ammonia into water, ASHRAE Trans. 97 (1) (1991) 204–213.
[46] H.-H. Lu, T.-Ch. Wu, Y.-M. Yang, J.-R. Maa, Transient heat and mass transfer in a drop experiencing absorption with internal circulation, Int. Commun. Heat Mass Transfer 25 (8) (1998) 1115–1126.
[47] M. Izquierdo, M. Venegas, M. de Vega, P. Rodríguez, Absorption cycles using low temperature heat for refrigeration and heat pumps, in: Proceedings of the 2nd International Heat Powered Cycles Conference, Paris, 2001, pp. 101–108.

[48] M. Venegas, M. Izquierdo, M. de Vega, A. Lecuona, Thermodynamic study of multistage absorption cycles using low temperature heat, Int. J. Energy Res. 26 (8) (2002) 775–791.
[49] C.A. Infante Ferreira, Thermodynamic and physical property data equations for ammonia–lithium nitrate and ammonia–sodium thiocyanate solutions, Solar Energy 32 (2) (1984) 231–236.
[50] ASHRAE, Fundamentals Handbook, ASHRAE, Atlanta, 1993.
[51] IIAR, Ammonia Data Book, International Institute of Ammonia Refrigeration, Washington, DC, 1993.
[52] R. Kusaka, K. Ban, Y. Nakamura, S. Shimokawa, Diffusion of cations and solvent molecules in the concentrated $LiNO_3$–NH_3 system, J. Phys. Chem. 91 (1987) 985–987.
[53] A.H. Lefebvre, Atomization and Sprays, Hemisphere Publishing, 1989.
[54] L. Bayvel, Z. Orzechowski, Liquid Atomization, Taylor & Francis, USA, 1993.
[55] J.R. Welty, Ch.E. Wicks, R.E. Wilson, Fundamentos de transferencia de momento, calor y masa, Editorial Limusa, México, 1999.
[56] E. Costa Novella, Ingeniería Química 5, Transferencia de materia, Editorial Alhambra, Madrid, 1988.
[57] H.M. Habib, B.D. Wood, Simultaneous heat and mass transfer for a falling film absorber—the two phase flow problem, in: Solar Energy Engineering, Proceedings of 12th Annual Solar Energy Conference, ASME, 1990, pp. 61–67.
[58] R. Clift, J.R. Grace, M.E. Weber, Bubbles, Droplets, and Particles, Academic Press, New York, 1978.
[59] J. Happel, H. Brenner, Low Reynolds Number Hydrodynamics, Kluwer Academic Publishers, Netherlands, 1991.
[60] D.A. Anderson, J.C. Tannehill, R.H. Pletcher, Computational fluid mechanics and heat transfer, Taylor & Francis, 1984.
[61] M.A.I. El-Shaarawi, A. Al-Farayedhi, M.A. Antar, Boundary layer flow about and inside a liquid sphere, J. Fluids Eng., Trans. ASME 119 (1997) 42–49.
[62] MATLAB 5.3, The MathWorks, Nattick, MA, USA, 1999.
[63] M. Venegas, P. Rodríguez, A. Lecuona, M. Izquierdo, Spray absorbers in absorption systems using lithium nitrate–ammonia solution, in: Proceedings of Eurotherm Seminar No. 72, Valencia, 2003, pp. 19–24.
[64] M. Venegas, D. Arzoz, P. Rodríguez, M. Izquierdo, Heat and mass transfer in $LiNO_3$–NH_3 spray absorption system, Int. Commun. Heat Mass Transfer 30 (6) (2003) 805–815.